

Constraining the Dark Energy Equation of State with HII Galaxies

R. Chávez,^{1,2,3*} M. Plionis,^{4,5} S. Basilakos,⁶ R. Terlevich,^{1,7} E. Terlevich,¹
J. Melnick,⁸ F. Bresolin,⁹ and A.L. González-Morán¹

¹*Instituto Nacional de Astrofísica Óptica y Electrónica, AP 51 y 216, 72000, Puebla, México*

²*Cavendish Laboratory, University of Cambridge, 19 J. J. Thomson Ave, Cambridge CB3 0HE, UK*

³*Kavli Institute for Cosmology, University of Cambridge, Madingley Road, Cambridge CB3 0HA, UK*

⁴*Physics Dept., Aristotle Univ. of Thessaloniki, Thessaloniki 54124, Greece*

⁵*National Observatory of Athens, P.Pendeli, Athens, Greece*

⁶*Academy of Athens, Research center for Astronomy and Applied Mathematics, Soranou Efessiou 4, 11527, Athens, Greece*

⁷*Institute of Astronomy, University of Cambridge, Madingley Road, Cambridge CB3 0HA, UK*

⁸*European Southern Observatory, Alonso de Cordova 3107, Santiago, Chile*

⁹*Institute for Astronomy of the University of Hawaii, 2680 Woodlawn Drive, 96822 Honolulu, HI USA*

v18 — Compiled at 8:48 hrs on 18 February 2020

ABSTRACT

We use the HII galaxies $L-\sigma$ relation and the resulting Hubble expansion cosmological probe of a sample of just 25 high- z (up to $z \sim 2.33$) HII galaxies, in a joint likelihood analysis with other well tested cosmological probes (CMB, BAOs) in an attempt to constrain the dark energy equation of state (EoS). The constraints, although still weak, are in excellent agreement with those of a similar joint analysis using the well established SNIa Hubble expansion probe. Interestingly, even with the current small number of available high redshift HII galaxies, the HII/BAO/CMB joint analysis gives a 13% improvement of the quintessence dark energy cosmological constraints compared to the BAO/CMB joint analysis.

We have further performed extensive Monte Carlo simulations, with a realistic redshift sampling, to explore the extent to which the use of the $L-\sigma$ relation, observed in HII galaxies, can constrain effectively the parameter space of the dark energy EoS. The simulations predict substantial improvement in the constraints when increasing the sample of high- z HII galaxies to 500, a goal that can be achieved in reasonable observing times with existing large telescopes and state-of-the-art instrumentation.

Key words: galaxies: starburst – cosmology: dark energy – cosmological parameters

1 INTRODUCTION

The observational evidence for an accelerated cosmic expansion was first given by Type Ia Supernovae (SNIa) (Riess et al. 1998; Perlmutter et al. 1999). Since then, measurements of the cosmic microwave background (CMB) anisotropies (e.g. Jaffe et al. 2001; Pryke et al. 2002; Spergel et al. 2007; Planck Collaboration et al. 2015) and of Baryon Acoustic Oscillations (BAOs) (e.g. Eisenstein et al. 2005), in combination with independent Hubble parameter measurements (e.g. Freedman et al. 2012), have provided ample evidence of the presence of a dark energy (DE) component in the Universe.

To the present day, the main geometrical tracer of the

cosmic acceleration has been SNIa at redshifts $z \lesssim 1.5$ (e.g. Suzuki et al. 2012; Betoule et al. 2014). It is of great importance to use alternative geometrical probes at higher redshifts in order to verify the SNIa results and to obtain more stringent constraints in the cosmological parameters solution space (Plionis et al. 2011), with the final aim of discriminating among the various theoretical alternatives that attempt to explain the accelerated expansion of the Universe (cf. Suyu et al. 2012).

The $L(H\alpha) - \sigma$ relation between the velocity dispersion (σ) and Balmer-line luminosity ($L[H\alpha]$, usually HII) of HII galaxies has already proven its potential as a cosmological tracer (e.g. Melnick et al. 2000; Siegel et al. 2005; Plionis et al. 2011; Chávez et al. 2012, 2014; Terlevich et al. 2015, and references therein). It has been shown that the $L(H\beta) - \sigma$ relation can be used in the local Universe to con-

* E-mail: ricardo.chavez@mrao.cam.ac.uk

strain the value of H_0 (Chávez et al. 2012). At high- z it can set constraints on the parameters of the DE Equation of State (EoS) (Terlevich et al. 2015).

H II Galaxies are a promising tracer for the parameters of the DE EoS precisely because they can be observed, using the current available infrared instrumentation, up to $z \sim 3.5$ (cf. Terlevich et al. 2015). Even when their scatter on the Hubble diagram is about a factor of two larger than in the case of SNIa, this disadvantage is compensated by the fact that H II galaxies are observed to much larger redshifts than SNIa where the degeneracies for different DE models are substantially reduced (cf. Plionis et al. 2011).

In addition, because the $L(\text{H}\beta) - \sigma$ relation systematic uncertainty sources (Chávez et al. 2012, 2014) are not the same as those of SNIa, H II galaxies constitute an important complement to SNIa in the local Universe, contributing to a better understanding of the systematic errors of both empirical methods.

In this paper we perform an HII/BAO/CMB joint likelihood analysis and compare the resulting cosmological constraints with those of a BAO/CMB and a SNIa/BAO/CMB joint likelihood analysis (for the latter we use the *Union 2.1* SNIa compilation (Suzuki et al. 2012)).

Furthermore, we present extensive Monte-Carlo simulations, tailored to the specific uncertainties of the H II galaxies $L(\text{H}\beta) - \sigma$ relation and currently available instrumentation, to demonstrate its potential possibilities as a cosmological tracer to $z \lesssim 3.5$, to probe a region where the Hubble function is very sensitive to the variations of cosmological parameters (Melnick et al. 2000; Plionis et al. 2011).

The paper is organised as follows: in section 2 we succinctly describe the data used and associated systematic uncertainties; cosmological constraints that can be obtained from the data are explored in section 3; in section 4 we discuss the Monte-Carlo simulations, in section 5 we discuss the planned data acquisition in order to obtain better constraints on the cosmological parameters. Finally in section 6 we present our conclusions.

2 H II GALAXIES DATA

Our current sample consists of a low- z subsample of 107 H II galaxies ($0.01 \leq z \leq 0.16$) extensively analysed in Chávez et al. (2014) and 24 Giant Extragalactic H II Regions (GEHR) at $z \leq 0.01$ described in Chávez et al. (2012). The sample also includes a high- z subsample composed by 6 star-forming galaxies, selected from Hoyos et al. (2005); Erb et al. (2006b,a) and Matsuda et al. (2011), that we observed (Terlevich et al. 2015) using X-SHOOTER (Vernet et al. 2011) at the Very Large Telescope in Paranal. The data of 19 objects taken from Erb et al. (2006a); Maseda et al. (2014) and Masters et al. (2014) complete the sample. Altogether, the redshift range covered by the high- z subsample is $0.64 \leq z \leq 2.33$.

It has been demonstrated (cf. Terlevich & Melnick 1981; Melnick et al. 1988; Terlevich et al. 2003; Plionis et al. 2011; Chávez et al. 2012, 2014) that the $L(\text{H}\beta) - \sigma$ relation for H II galaxies and GEHR can be used to measure distances via the determination of their Balmer emission line luminosity, $L(\text{H}\beta)$, and the velocity dispersion (σ) of the young starforming cluster from measurements of

Table 1. Systematic error budget on the distance moduli, μ . The typical uncertainty contribution of each source of systematic error is given.

Source	Error
Size of the Burst	0.175
Age of the burst	0.05
Abundances	0.05
Extinction	0.175
Total	0.257

the line width. The relevant relation can be expressed as:

$$\log L(\text{H}\beta) = (5.05 \pm 0.097) \log \sigma(\text{H}\beta) + (33.11 \pm 0.145). \quad (1)$$

Distance moduli are then obtained from:

$$\mu^\circ = 2.5 \log L(\text{H}\beta)_\sigma - 2.5 \log f(\text{H}\beta) - 100.195 \quad (2)$$

where $L(\text{H}\beta)_\sigma$ is the luminosity estimated from the $L(\text{H}\beta) - \sigma$ relation as in eq. (1) and $f(\text{H}\beta)$ is the measured flux in the $\text{H}\beta$ line. The uncertainty on the distance moduli, σ_{μ° , is propagated from the uncertainties in σ_i and f_i and the slope and intercept of the distance estimator in eq. (1).

2.1 Systematic Errors

2.1.1 Size of the burst

The scatter found in the $L(\text{H}\beta) - \sigma$ relation for H II galaxies suggests a dependence on a second parameter (cf. Terlevich & Melnick 1981; Melnick et al. 1987). Indeed Chávez et al. (2014), using SDSS DR7 effective Petrosian radii, corrected for seeing, for a sample of local H II galaxies, found the size of the starforming region to be this second parameter.

For the high- z samples, unfortunately, we do not have any size measurements, so using it as a second parameter in the correlation is impossible. The error induced by not using the size of the burst as a second parameter appears in the uncertainties in the slope and zero point of the $L(\text{H}\beta) - \sigma$ relation, i.e. our uncertainty values already incorporate this effect. In Table 1 we show the typical contribution of the size of the burst to the uncertainty on the distance moduli.

2.1.2 Age of the burst

Melnick et al. (2000) have demonstrated that H II galaxies with equivalent width of $\text{H}\beta$, $W(\text{H}\beta) < 25 \text{ \AA}$, do follow an $L(\text{H}\beta) - \sigma$ relation with a similar slope but different intercept than those with larger $W(\text{H}\beta)$, i.e. older starbursts follow a parallel less luminous $L(\text{H}\beta) - \sigma$ relation. For the study presented here, the starburst age is a controlled parameter in the sense that we have selected our sample to be composed of very young objects ($\lesssim 5 \text{ Myr}$, for instantaneous burst models cf. Leitherer et al. 1999) by putting a high lower limit to the value of $W(\text{H}\beta) > 50 \text{ \AA}$. Therefore only the youngest bursts were considered and in this way the effects of the age of the burst as a systematic error on the $L(\text{H}\beta) - \sigma$ relation has been minimised; this selection also minimises the contamination by an older underlying stellar component.

We have demonstrated (Chávez et al. 2014) that using the $W(\text{H}\beta)$ as a second parameter in the $L(\text{H}\beta) - \sigma$ correlation reduces only slightly the scatter because of the small dynamic range of the age of our sample objects. We chose (Terlevich et al. 2015) not to use the $W(\text{H}\beta)$ as a parameter to ‘correct’ the $L(\text{H}\beta) - \sigma$ relation. Therefore, the small effect of the age of the burst on the correlation manifests itself in the uncertainties of the slope and zero point of the $L(\text{H}\beta) - \sigma$ relation that we are adopting. In Table 1 we show the typical contribution of the age of the burst to the uncertainty on the distance moduli.

2.1.3 Abundances

The oxygen abundance of HII galaxies was considered in the past (eg. Melnick et al. 1987, 2000; Siegel et al. 2005) as a second parameter for the $L(\text{H}\beta) - \sigma$ relation. We have explored again this issue in Chávez et al. (2014) for our local sample and concluded that the effect albeit present is very small.

We chose (Terlevich et al. 2015) not to use the oxygen abundance as a parameter to ‘correct’ the $L(\text{H}\beta) - \sigma$ relation, and thus the small effect of the metallicity of the burst on the correlation is already part of the uncertainties of the slope and zero point of the $L(\text{H}\beta) - \sigma$ relation that we are adopting. The typical contribution of the abundances to the uncertainty on the distance moduli is shown in Table 1.

2.1.4 Extinction

The internal extinction correction was performed on the low- z subsample following the procedure described in Chávez et al. (2014) and using the extinction coefficients derived from SDSS DR7 spectra. For the high- z subsample we used the extinction coefficients given in the literature (Erb et al. 2006b,a; Matsuda et al. 2011; Maseda et al. 2014; Masters et al. 2014). Typical contribution of the extinction to the distance modulus uncertainty is also shown in Table 1.

2.1.5 Malmquist bias

The Malmquist bias is a selection effect in flux limited samples. Due to the preferential detection of the most luminous objects as a function of distance and limiting flux, at any distance there are always more faint objects being randomly scattered-in of the flux-limited sample than bright objects being randomly scattered-out of the sample. Therefore the source mean absolute magnitude at some large distance will be systematically fainter than what expected due to the flux limit of the catalogue at that distance.

The Malmquist bias for our flux limited low- z calibrating sample was calculated following the procedure given by Giraud (1987). In the first place, using the Luminosity Function for HII galaxies (Chávez et al. 2014) we estimated the expected value of the luminosity at any redshift as:

$$\langle L \rangle = \frac{\int_{L_i}^{L_s} L^\alpha L dL}{\int_{L_i}^{L_s} L^\alpha dL}, \quad (3)$$

where $L_i = 10^{39.7}$ is the lower limit of the luminosity function, $L_s = 10^{42.5}$ is the upper limit and $\alpha = -1.5$ is the slope (Chávez et al. 2014).

Subsequently, at each z we calculate the luminosity expected when we change the lower limit of the Luminosity Function to the value given by the flux limit at that redshift:

$$\langle L(z) \rangle = \frac{\int_{L_l(z)}^{L_s} L^\alpha L dL}{\int_{L_l(z)}^{L_s} L^\alpha dL}, \quad (4)$$

where the value of $L_l(z)$ can be calculated from:

$$\log L_l(z) = \log f_l + 2 \log(d_L[z, \mathbf{p}]) + 50.08, \quad (5)$$

where $\log f_l = -14.3$ is the flux limit of our low- z sample and d_L is the luminosity distance as function of z and a set of cosmological parameters \mathbf{p} .

Finally the bias is a function of the difference of the unbiased and biased expected values of the luminosity and can be obtained as:

$$b(\log L_\mu) = \frac{\sigma_0^2}{\sigma_{L_0}^2 + \sigma_0^2} (\log \langle L \rangle - \log \langle L(z) \rangle) \quad (6)$$

where σ_0 is the dispersion of residuals of the $L(\text{H}\beta) - \sigma$ relation and σ_{L_0} is the dispersion of the distribution of luminosities in the sample. From the above equation the bias for a certain distance modulus can be obtained as $b(\mu) = 2.5b(\log L_\mu)$.

The typical value of the Malmquist bias found for our low- z calibrating sample is $b(\mu) = 0.03$, extremely small compared to the other uncertainties.

2.2 Gravitational Lensing Effects

Details of the expected effect of gravitational lensing on the distance modulus of high- z standard candles (e.g. Holz & Wald 1998; Holz & Linder 2005; Brouzakis & Tetradis 2008, and references therein) were given in Plionis et al. (2011). The basic assumption used in developing a correction procedure for this effect is that the magnification distribution resembles a lognormal with zero mean (the mean flux of each source over all possible different paths is conserved, since lensing does not affect photon numbers), a mode shifted towards the de-magnified regime and a long tail towards high magnification. This sort of distribution has been found in analyses based on Monte-Carlo procedures and ray-tracing techniques (cf. Holz & Linder 2005).

Therefore most high- z sources will be demagnified (will appear artificially fainter), inducing an apparently enhanced accelerated expansion, while a few will be highly magnified. The effect is obviously stronger for higher redshift sources since the lower the redshift the smaller the optical depth of lensing.

It is important to note that the effect of gravitational lensing is not only to increase the distance modulus uncertainty, which is proportional to the redshift, but also to induce a systematic shift of the mode of the distance modulus distribution to de-magnified (fainter) values. These effects appear to be independent of the underlying cosmology and the details of the density profile of cosmic structures (eg. Wang et al. 2002).

A procedure, first suggested by Holz & Linder (2005), to correct statistically for such an effect was explained in detail in Plionis et al. (2011). The reader is referred to that work. We apply this procedure to our analysis of the Hubble expansion cosmological probe, using either H II galaxies or SNIa, but find minimal effects on the resulting cosmological parameter constraints.

3 COSMOLOGICAL CONSTRAINTS

A variety of observational probes have been developed through the years in order to provide constraints on the cosmological parameters, which in turn determine the specifics of the evolution of the Universe. These probes may be divided in two general classes; *geometrical* and *dynamical* and both use the redshift dependence of the comoving distance to a source:

$$d_C(z) = \int_0^z \frac{cdz'}{H(z')}, \quad (7)$$

where the Hubble function $H(z)[\equiv H_0 E(z)]$ is derived from the first Friedman equation and $E(z)$ is given in the matter-dominated era for a flat Universe with matter and DE, by:

$$E^2(z) = \left[\Omega_{m,0}(1+z)^3 + \Omega_{w,0}(1+z)^{3y} \exp\left(\frac{-3w_a z}{z+1}\right) \right] \quad (8)$$

with $y = (1 + w_0 + w_a)$. The parameters w_0 and w_a refer to the DE equation of state, the general form of which is:

$$p_w = w(z)\rho_w, \quad (9)$$

with p_w the pressure and ρ_w the density of the postulated DE fluid. Different DE models have been proposed and many are parametrized using a Taylor expansion around the present epoch:

$$w(a) = w_0 + w_a(1-a) \implies w(z) = w_0 + w_a \frac{z}{1+z}, \quad (10)$$

(CPL model; Chevallier & Polarski 2001; Linder 2003; Peebles & Ratra 2003; Dicus & Repko 2004; Wang & Mukherjee 2006). The cosmological constant is just a special case of DE, given for $(w_0, w_a) = (-1, 0)$, while the so called *quintessence* (QDE) models are such that $w_a = 0$ but w_0 can take values $\neq -1$.

Therefore, assuming a flat Universe ($\Omega_m + \Omega_w = 1$), a negligible radiation density parameter and the generic CPL DE EoS parametrisation, the most general set of cosmological parameters that is necessary to be constrained in order to define the actual cosmological model, is given by $\mathbf{p} = \{\Omega_{m,0}, w_0, w_a\}$. Note that we do not include as a parameter the Hubble constant because, as it will become clear further below, the dependence on H_0 is factored out. In what follows, we will consider two parametrisation of the DE EoS, assuming a flat Universe, i.e.,

- (i) QDE model with $\mathbf{p} = \{\Omega_{m,0}, w_0, 0\}$, and
- (ii) CPL model with $\mathbf{p} = \{\Omega_{m,0}, w_0, w_a\}$

The *geometrical* probes, which are independent of the underline gravity theory, are used to probe the Hubble function through the redshift dependence of the luminosity, $d_L(z)$, or the angular diameter, $d_A(z)$, distance.

These methods utilize extragalactic sources for which

their luminosity is either known a priori (e.g. standard candles) or it can be estimated by using a distance-independent observational parameter. Alternatively, they can use cosmic phenomena for which their metric size is known (e.g. standard rulers). Then the cosmic expansion history is traced via the luminosity distance $d_L(z)$, in the first case, or the angular diameter distance $d_A(z)$, in the second case. To date such observations probe the integral of the Hubble expansion rate $H(z)$ either up to redshifts of order $z \simeq 1.5$ (e.g., SNIa, BAO, clusters), or at the redshift of recombination, $z_{rec} \sim 1100$ (CMB fluctuations).

Dynamical probes, on the other hand, map the expansion history based on measures of the growth rate of cosmological perturbations and therefore depend on the theory of gravity (cf. Bertschinger 2006; Nesseris & Perivolaropoulos 2008; Basilakos et al. 2013, and references therein). Such methods are also confined to relatively low redshifts, up to $z \simeq 1$.

It is therefore clear that the redshift range $1.5 \lesssim z \lesssim 1000$ is not directly probed to date by any of the above cosmological tests, and as discussed in Plionis et al. (2011) the redshift range $1.5 \lesssim z \lesssim 3.5$ is of crucial importance to constrain the DE EoS, since different DE models manifest their largest deviations in this redshift range. Therefore the fact that H II galaxies can be observed relatively easily at such redshifts make them ideal and indispensable tools for cosmological studies. Below we present the basics of the two *geometrical* probes that are extensively used to constrain the DE EoS parameters.

3.1 Standard Candle Probes

As discussed previously, for standard candle probes we need to use the luminosity distance of the sources tracing the Hubble expansion, given by $d_L = (1+z)d_C$. For convenience, which will be understood below, we define a further parameter, independent of the Hubble constant, by:

$$D_L(z, \mathbf{p}) = (1+z) \int_0^z \frac{dz'}{E(z', \mathbf{p})}. \quad (11)$$

i.e., $d_L = cD_L/H_0$. Using the luminosity distance, as calculated from a set of cosmological parameters, \mathbf{p} , and the redshift, z , we can obtain the ‘theoretical’ distance modulus of a source as:

$$\mu_{th} = 5 \log d_L(\mathbf{p}, z) + 25 = 5 \log D_L(\mathbf{p}, z) + \mu_0, \quad (12)$$

where $\mu_0 = 42.384 - 5 \log h$. Therefore, to restrict a given set of cosmological parameters, we define the usual χ^2 minimisation function as:

$$\chi_{sc}^2(\mathbf{p}) = \sum_{i=1}^N \frac{[\mu_{obs}(z_i) - \mu_{th}(z_i, \mathbf{p})]^2}{\sigma_{\mu,i}^2}, \quad (13)$$

where N is the total number of sources used, the suffix *sc* indicates the standard candle probe and $\mu_{obs}(z_i)$ and $\sigma_{\mu,i}^2$ are the distance moduli and the corresponding uncertainties at the observed redshift z_i . Inserting the second equality of eq.(12) into eq.(13) we find after some simple algebra that

$$\chi_{sc}^2(\mathbf{p}) = A(\mathbf{p}) - 2B(\mathbf{p})\mu_0 + C\mu_0^2, \quad (14)$$

where

$$A(\mathbf{p}) = \sum_{i=1}^N \frac{[\mu_{obs}(z_i) - 5 \log D_L(z_i, \mathbf{p})]^2}{\sigma_{\mu,i}^2},$$

$$B(\mathbf{p}) = \sum_{i=1}^N \frac{\mu_{\text{obs}}(z_i) - 5 \log D_L(z_i, \mathbf{p})}{\sigma_{\mu,i}^2},$$

$$C = \sum_{i=1}^N \frac{1}{\sigma_{\mu,i}^2}.$$

Obviously for $\mu_0 = B/C$ eq.(14) has a minimum at

$$\tilde{\chi}^2(\mathbf{p}) = A(\mathbf{p}) - \frac{B^2(\mathbf{p})}{C}. \quad (15)$$

Therefore, instead of using χ^2 we now minimise $\tilde{\chi}^2$ which is independent of μ_0 and thus of the value of the Hubble constant. For more details concerning the above treatment the reader is referred to [Nesseris & Perivolaropoulos \(2005\)](#).

3.2 Standard Ruler Probes

The first standard ruler probe is provided by the first peak of the CMB temperature perturbation spectrum, appearing at l_1^{TT} , which refers to the angular scale of the sound horizon at the last scattering surface, $\theta_1^{TT} \sim 1/l_1^{TT}$. Then by calculating its comoving scale, $r_s(z_{\text{rec}})$, we can derive its angular diameter distance by:

$$d_A(z_{\text{rec}}, \mathbf{p}) = \frac{r_s(z_{\text{rec}}, \mathbf{p})}{\theta_1^{TT}} = \frac{d_C(z_{\text{rec}}, \mathbf{p})}{1 + z_{\text{rec}}}. \quad (16)$$

Since the above equation is model dependent, through the CMB physics determination of r_s , a model independent parameter has been defined, the so-called *shift parameter* ([Bond et al. 1997](#); [Nesseris & Perivolaropoulos 2007](#)), which is the ratio of the position of the first peak to that of a reference model, and for spatially flat models it is given by:

$$R(\mathbf{p}) = \sqrt{\Omega_{m,0}} \int_0^{z_{\text{rec}}} \frac{dz}{E(z, \mathbf{p})}. \quad (17)$$

The observationally measured shift parameter, according to the recent *Planck* data ([Shafer & Huterer 2014](#)) is $R = 1.7499 \pm 0.0088$ at the redshift of decoupling (viz. at the last scattering surface, $z_{\text{rec}} = 1091.41$). At this point we would like to remind the reader that when dealing with the CMB shift parameter we need to include also the radiation density term in the $H(z)$ function since at recombination it amounts to $\sim 23\%$ of the matter density ($\Omega_{r,\text{rec}} \simeq 0.23\Omega_{m,\text{rec}}$) and therefore cannot be ignored. The final minimisation function is:

$$\chi_{\text{CMB}}^2(\mathbf{p}) = \frac{[R(\mathbf{p}) - 1.7499]^2}{0.0088^2}. \quad (18)$$

The second standard ruler probe that we use is the Baryonic Acoustic Oscillation (BAO) scale, a feature produced in the last scattering surface by the competition between the pressure of the coupled baryon-photon fluid and gravity. The resulting sound waves leave an overdensity signature at a certain length scale of the matter distribution. This length scale is related to the comoving distance that a sound wave can travel until recombination and in practice it manifests itself as a feature in the correlation function of galaxies on large scales ($\sim 100 h^{-1}$ Mpc). In recent years, measurements of the BAO have proven extremely useful as a ‘‘standard ruler’’. The BAOs were clearly identified, for the first time, as an excess in the clustering pattern of the SDSS luminous red galaxies ([Eisenstein et al. 2005](#)), and of the 2dFGRS galaxies ([Cole et al. 2005](#)). Since

then a large number of dedicated surveys have been used to measure BAOs, among which the WiggleZ Dark Energy Survey ([Blake et al. 2011](#)), the 6dFGS ([Beutler et al. 2011](#)) and the SDSS Baryon Oscillation Spectroscopic Survey (BOSS) of SDSS-III ([Eisenstein et al. 2011](#); [Anderson et al. 2014](#); [Aubourg et al. 2015](#)).

In the current paper we utilise the results of [Blake et al. \(2011, see their Table 3\)](#) which are given in terms of the acoustic parameter $A(z)$, first introduced by [Eisenstein et al. \(2005\)](#):

$$A(z_i, \mathbf{p}) = \frac{\sqrt{\Omega_{m,0}}}{[z_i^2 E(z_i, \mathbf{p})]^{1/3}} \left[\int_0^{z_i} \frac{dz'}{E(z', \mathbf{p})} \right]^{2/3} \quad (19)$$

with z_i the redshift at which the signature of the acoustic oscillations has been measured. The corresponding minimisation function is given by

$$\chi_{\text{BAO}}^2(\mathbf{p}) = \sum_{i=1}^6 \frac{[A(z_i, \mathbf{p}) - A_{\text{obs},i}]^2}{\sigma_i^2}. \quad (20)$$

where $A_{\text{obs},i}$ are the observed A_i values at six different redshifts, z_i , provided in [Blake et al. \(2011\)](#).

3.3 Joint Analysis of Different Probes

In order to place tight constraints on the corresponding parameter space of the DE EoS, the cosmological probes described previously must be combined through a joint likelihood analysis, given by the product of the individual likelihoods according to:

$$\mathcal{L}_{\text{tot}}(\mathbf{p}) = \prod_{i=1}^n \mathcal{L}_i(\mathbf{p}) \quad (21)$$

where n is the total number of cosmological probes used¹. This translates to an addition for the corresponding joint total χ_{tot}^2 function:

$$\chi_{\text{tot}}^2(\mathbf{p}) = \sum_{i=1}^n \chi_i^2(\mathbf{p}). \quad (22)$$

In our current analysis we sample the cosmological parameter space with the following resolution: $\delta\Omega_{m,0} = 0.001$, $\delta w_0 = 0.003$ and $\delta w_a = 0.016$. Also, the reported uncertainties for each unknown parameter of the vector \mathbf{p} are estimated after marginalising one parameter over the other, such that $\Delta\chi^2 (\leq 2\sigma)$. Note however that in order to appreciate the possible degeneracy among the different fitted parameters one must inspect the two-dimensional likelihood contours.

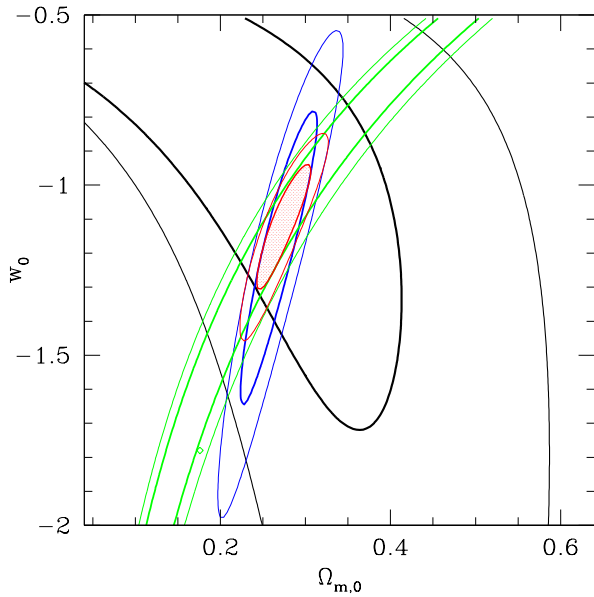
3.4 Results of the Joint Analysis

As discussed earlier our present sample of HII galaxies is dominated by the very-low redshift regime ($z < 0.15$) as it contains only a small number of high- z sources; therefore the cosmological constraints that can be imposed are very weak (see [Terlevich et al. 2015](#)). Nevertheless by joining the HII galaxy analysis with other cosmological probes we can

¹ Likelihoods are normalised to their maximum values.

Table 2. Cosmological parameters from the joint analysis of different combinations of probes and for both parameterisations of the DE EoS.

Probes	$\Omega_{m,0}$	w_0	w_a	χ_{min}^2	df
QDE parameterisation					
BAO/CMB	0.274 ± 0.0145	-1.109 ± 0.082	0	1.036	6
HII/BAO/CMB	0.278 ± 0.0143	-1.088 ± 0.080	0	213.85	162
SNIa/BAO/CMB	0.287 ± 0.0130	-1.034 ± 0.056	0	563.68	586
CPL parameterisation					
BAO/CMB	0.278	-1.052 ± 0.083	-0.112 ± 0.35	1.087	6
HII/BAO/CMB	0.278	-0.992 ± 0.084	-0.368 ± 0.38	213.72	162
SNIa/BAO/CMB	0.278	-0.983 ± 0.057	-0.304 ± 0.28	563.90	586

**Figure 1.** Likelihood contours for $\Delta\chi^2 = \chi_{tot}^2 - \chi_{tot,min}^2$ equal to 2.32 and 6.18 corresponding to the 1σ and 2σ confidence levels in the $(\Omega_{m,0}, w)$ plane. Results based on the H II galaxies are shown in black, on the CMB shift parameter (green) and on BAO (blue) while the joint contours are shown in red.

further test the effectiveness of using H II galaxies as alternative tracers of the Hubble expansion. To this end we will present and compare our results of the joint analysis but using as standard candles separately our H II galaxies and the SNIa.

In Figure 1 we present the 1σ and 2σ likelihood contours in the $(\Omega_{m,0}, w)$ plane for the following probes: H II galaxy Hubble relation (black contours), CMB shift parameter (green) and BAO (blue), whereas with red we present the result of the joint analysis. The solution provided by the H II galaxy Hubble relation probe has been shown to be consistent with that of the SNIa, albeit leaving mostly unconstrained the QDE free parameters (Terlevich et al. 2015). However, the joint analysis reduces dramatically the solution space, providing quite stringent constraints on the two QDE parameters. Even with the current very broad H II-galaxy likelihood contours, the joint HII/BAO/CMB analysis increases the Figure of Merit (FoM) by 13% with respect to that of the BAO/CMB joint analysis alone.

In order to compare the performance of the H II galax-

ies (as they stand today in our sample of only 25 high- z sources) with that of the *Union2.1* SNIa, we display in Figure 2 the joint likelihood contours for HII/BAO/CMB_{shift} (black contours), and SNIa/BAO/CMB_{shift} (red contours) probes for both DE EoS parameterisations. Note that in the case of the CPL analysis we impose an *a priori* value for the cosmological matter density parameter, $\Omega_{m,0} = 0.278$, and allow the two DE EoS parameters, w_0 and w_a to vary.

A first observation is that both joint analyses, based either on H II galaxies or SNIa, provide consistent results for both DE equation of state parameterisations, although (as expected) the SNIa rate better since the SNIa sample is much larger and their median redshift is significantly higher than that of our preliminary H II galaxy sample. For the QDE case, the broad H II galaxy likelihood contours and the corresponding extensive parameter degeneracy is reduced significantly with the joint HII/BAO/CMB analysis, while the degeneracy appears to disappear with the SNIa/BAO/CMB analysis. As expected for the more demanding CPL parameterisation the degeneracy between w_0 and w_a is present in both sets of joint analyses. However, what is particularly interesting is that for the CPL model the two joint analyses provide the same minimum, as can be seen also in Table 2, where we list the resulting cosmological parameters and their uncertainties for the different combinations of cosmological probes.

It is very encouraging that even with the current H II galaxy pilot sample, the combined analysis of the H II data with BAOs and the CMB shift parameter provides constraints on the cosmological parameters which are in agreement with those of the joint SNIa/BAOs/CMB_{shift}.

We plan to considerably increase the current sample of high- z H II galaxies (see next section) which together with other future cosmological data, based for example on *Euclid*, will improve significantly the relevant constraints (especially on w_a) and thus the validity of a running EoS parameter, namely $w(z)$, will be effectively tested.

4 MONTE-CARLO SIMULATIONS

In order to predict the effectiveness of using high- z H II galaxies to constrain the DE EoS, we have performed an extensive series of Monte-Carlo simulations with which we assess our ability to recover the input parameters of an *a priori* selected cosmological model, in our case that of the concordance cosmology $(\Omega_{m,0}, w_0, w_a) = (0.28, -1, 0)$. We distribute different numbers of mock high- z H II galaxies in

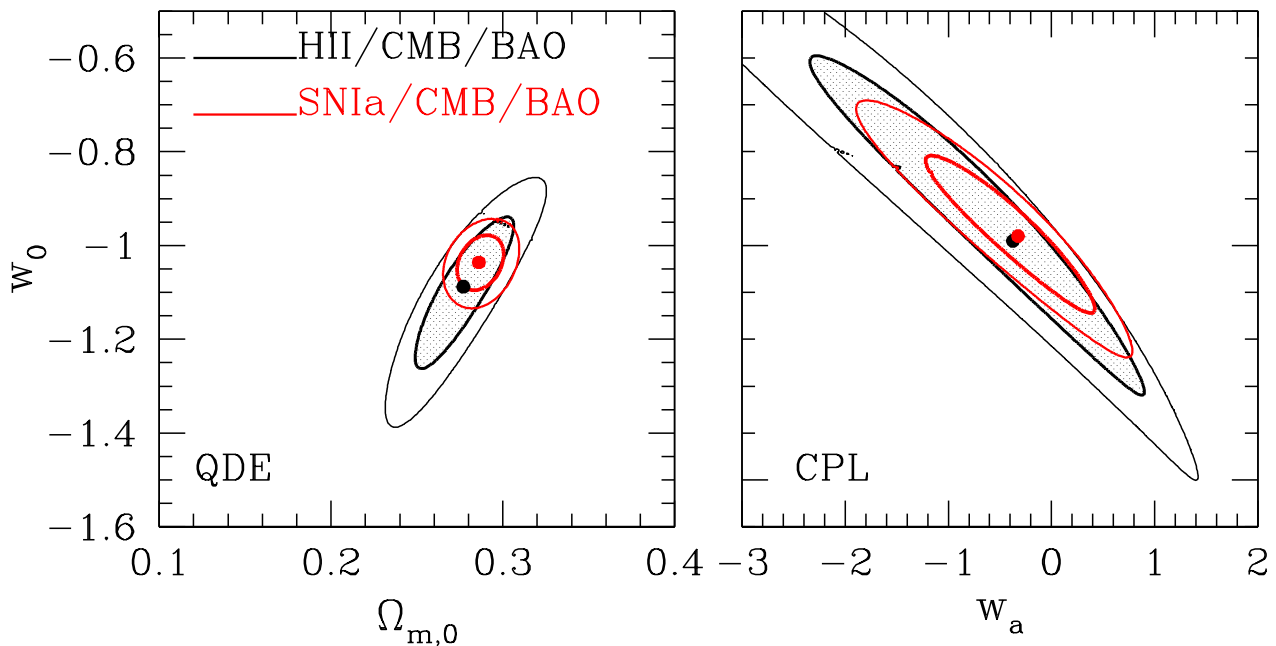


Figure 2. Comparison of the joint likelihood contours of the HII/CMB/BAO (black contours) and of the SNIa/CMB/BAO (red contours) probes. *Left Panel:* QDE dark energy equation of state parametrization. *Right Panel:* CPL dark energy equation of state parametrization using $\Omega_{m,0} = 0.278$ as a prior.

redshift according to the observational constraints of the adequate, for our purpose, instruments and telescopes (in this case the VLT-KMOS spectrograph at ESO²). The range of the available near IR bands for this instrument are shown in Table 3, as well as the corresponding redshift ranges within which either the H α or [OIII] emission lines can be observed. There are practically 4 independent redshift ranges that can be sampled centered at $\langle z \rangle \simeq 0.8, 1.4, 2.3$ and 3.3 , and these are the redshift ranges where we will distribute our mock high- z H II galaxies³. Since the IR bands window function are clearly not top-hat, we model the distribution of redshifts, within each z -window, by a Gaussian with mean and standard deviation given in Table 3.

The Monte-Carlo simulation procedure that we follow entails assigning to each mock H II galaxy the ideal distance modulus for the selected cosmology and an uncertainty which is determined by the expected distribution of luminosity and flux errors that enter in the relation (2). We then transform these errors in a distance modulus error distribution and use this distribution to assign randomly errors to each high- z mock H II galaxy. The mean distance modulus uncertainty is thus derived from propagating the mean

² As we prepared this work, we have also procured some 25 high- z H II galaxies data with MOSFIRE at Keck. A paper is in preparation.

³ Note that other studies that present simulations of the constraints provided by future high- z tracers of the Hubble expansion do not always take into account the limited redshift intervals that can be observationally probed (cf. Scovacricchi et al. 2016).

Table 3. The KMOS FWHM sensitivities and redshift windows

Band	λ /nm	H α z -window	[OIII] z -window	Exp.time (sec)
J	1175 \pm 40	0.79 \pm 0.026	1.35 \pm 0.046	$S/N \simeq 25$ 1800
H	1635 \pm 65	1.49 \pm 0.060	2.26 \pm 0.090	1500
K	2145 \pm 65	2.26 \pm 0.070	3.28 \pm 0.100	2100

The width of the wavelength coverage includes only the region with sensitivity higher than 50% of the band peak sensitivity.

velocity dispersion and flux errors via eq.(2), i.e.:

$$\sigma_{\mu} = 2.5 \left(\log \sigma^2 \sigma_a^2 + a^2 \sigma_{\log \sigma}^2 + \sigma_b^2 + \frac{\sigma_f^2}{\ln(10)^2 f^2} \right)^{1/2} \quad (23)$$

where a and b are the slope and intercept of the $L_{H\beta} - \sigma$ relation, σ_a and σ_b are the corresponding uncertainties of the fit, while f and σ_f are the $H\beta$ line flux and its uncertainty. Assuming a flux uncertainty of $\lesssim 10\%$ (as indeed we find for the three $z \gtrsim 1.5$ H II galaxies we observed with X-SHOOTER; see Terlevich et al. 2015) and the uncertainties of our $L_{H\beta} - \sigma$ relation, we obtain a mean $\langle \sigma_{\mu} \rangle \simeq 0.6$ mag, slightly lower than the measured values of our low- z sample ($\langle \sigma_{\mu} \rangle \simeq 0.7$ mag).

The available high- z H II galaxy data from the literature (as well as our own data) indicate a large dispersion of the distance modulus uncertainty and therefore, for the purpose of our simulations, we will assume a Gaussian uncertainty distribution with mean $\langle \sigma_{\mu} \rangle \simeq 0.6$ mag and a standard deviation of $\sigma_{\sigma} \simeq 0.24$. Obviously, the outcome of the simula-

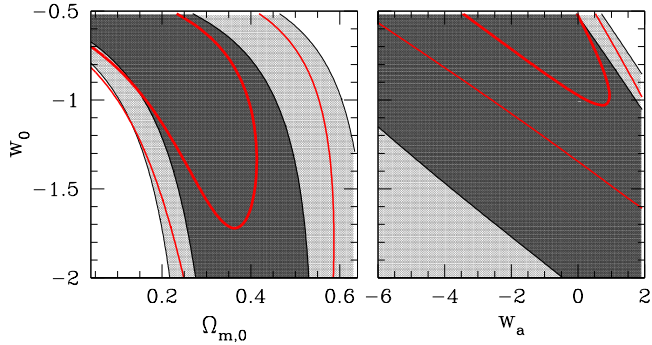


Figure 3. Likelihood contours corresponding to the 1σ and 2σ confidence levels for our H II galaxy sample but using the ideal concordance cosmology distance moduli (grey-scale contours). In red we show the corresponding true constraints of our current sample. *Left Panel:* QDE parametrization. *Right Panel:* CPL parametrization with $\Omega_{m,0} = 0.278$.

tions are sensitive to the error distribution and the results presented here are intended as indicative of the potential of our approach.

4.1 Results of simulations

In order to test the effectiveness of our procedure, as a starting point, we assign to each of the 156 H II galaxies and GEHR of our high-quality velocity dispersions observational sample (Chávez et al. 2014; Terlevich et al. 2015) the ideal distance modulus and the actual observed uncertainty. We then perform our usual χ^2 minimisation procedure and derive the cosmological constraints, shown in Figure 3 as greyscale contours. We also overplot the corresponding true observational constraints of the same H II galaxy sample, which are statistically consistent with the *ideal* case (more so for the QDE parametrization). If for the *ideal* distance modulus case we assign to each source the model observational uncertainties, discussed previously, we obtain similar constraints as in the true uncertainties case but with slightly higher FoM, by a factor of $\lesssim 2$.

For our tests we will consistently estimate the increase of the current FoM, based on the 156 H II galaxies and GEHR of our sample using the *ideal* distance moduli with that provided when we add different numbers of high- z H II galaxies, distributed in the redshift ranges shown in Table 3. This exercise will be presented for both the QDE and CPL parameterisations of the DE EoS. Note that the distribution of numbers of the mock H II galaxies at the different redshift ranges could also affect the results in the sense that different cosmological models show the largest deviations from the concordance model at different redshifts (eg., Fig.1 of Plionis et al. 2011). After a trial and error procedure we found that an optimal distribution of the fractions of the total number of high- z H II galaxies in the 4 available redshift ranges, shown in Table 3, is 0.2, 0.2, 0.3 and 0.3 (from the lowest to the highest redshift range). However, the case of equal fraction among the different redshifts provide similar results.

We performed 100 Monte-Carlo realisations for each se-

lected number of mock high- z H II galaxies, and the aggregate results are presented in Figure 4, in the form of the ratio between the simulation FoM and that of our current sample of H II galaxies. Thus what is shown is the factor by which the FoM increases with respect to its current value. This factor increases linearly with N_{HII} providing the following rough analytic expressions:

$$F_{\text{QDE}} \simeq 0.015N_{\text{HII}} + 1.72 \quad \text{and} \quad F_{\text{CPL}} \simeq 0.004N_{\text{HII}} + 1.51$$

which means that for the very realistic near future expectations of observations of ~ 500 high- z H II galaxies, we predict a \sim ten-fold increase of the current FoM for the QDE parameterisation and \sim four-fold increase of the corresponding FoM for the CPL parameterisation, within the limits of the parameters shown in Figure 4.

As an example, we present in Figure 5 the results of one simulation of 500 high- z mock H II galaxies both for the QDE and CPL parameterisations of the DE EoS (greyscale contours), which can be compared with the constraints of our current sample (but using for consistency the ideal distance moduli).

5 FEASIBILITY OF THE PROJECT AND FUTURE WORK

The realisation of this project relies on two main prerequisites; finding an adequate number of high- z H II galaxy targets and being able to observe them using a reasonable amount of observing time.

To this end, we compiled a sample of objects searching the literature for high- z H II galaxy candidates that we define as compact emission line systems with either $W(\text{H}\alpha) > 200 \text{ \AA}$ and $W[\text{OIII}]\lambda 5007 > 200 \text{ \AA}$ or with $W(\text{H}\beta) > 50 \text{ \AA}$ and $\text{FWHM} < 150 \text{ \AA}$ and with $z > 1.2$. We have found up to now more than 500 candidates in about 20 high galactic latitude fields (González-Morán et al. in preparation). To estimate the feasibility of our project we calculated the time it could take to observe the whole sample. For this estimate we have assumed the use of IR spectroscopic facilities with resolution R larger than 4000 in 10m class telescopes and with multiplexing capability. These facilities are at present only two, KMOS at the VLT and MOSFIRE at Keck. We have used the KMOS Exposure Time Calculator to estimate the time needed to obtain a S/N 25 or larger in either H α or [OIII] $\lambda 5007$ for the faintest objects in our list and combine this estimate with their surface density at $z \sim 2.3$. The typical exposure times are about 3 hours per field. Each search field is typically populated by 25 objects with about 8 to 15 simultaneously inside either the KMOS or MOSFIRE field of view. Thus the number of objects that can be observed in a 10 hours night ranges from 24 to 45, therefore about 15 observing nights would be needed to observe 500 H II galaxies. This estimate is shown in the upper scale of Figure 4.

6 CONCLUSIONS

We have used the Hubble relation of H II galaxies in a joint likelihood analysis with the BAO and CMB cosmological probes with the aim of testing the consistency of

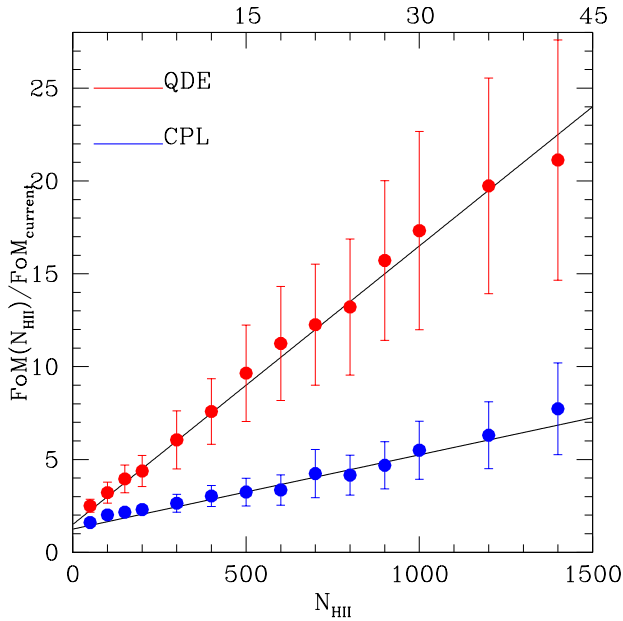


Figure 4. The factor by which the FoM of the QDE and CPL EoS constraints increases with respect to its current value (based on the observed 25 high- z HII galaxies) as a function of the number of mock high- z HII galaxies. The FoM has been estimated within the limits of the parameters shown in Figure 3. The red and blue points correspond to the QDE and CPL parameterisations of the DE EoS, respectively. The solid black lines are the linear fits to the corresponding coloured curves. The scale at the top gives the number of 10m class telescope nights needed in order to observe 500, 1000 and 1500 objects as 15, 30 and 45 nights respectively.

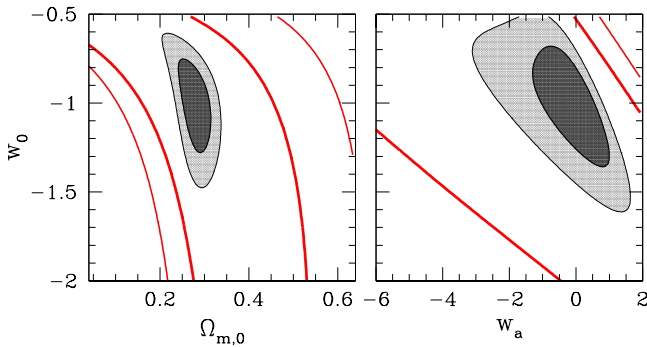


Figure 5. Likelihood contours corresponding to the 1σ and 2σ confidence levels for our HII galaxy sample but adding 500 high- z mock HII galaxies (grey-scale contours). In red we show the corresponding current constraints (ie., without the high- z mock HII galaxies). We consistently use the *ideal* distance moduli of the concordance cosmology. *Left Panel:* QDE parametrisation. *Right Panel:* CPL parametrisation using $\Omega_{m,0} = 0.278$.

the derived cosmological constraints with those of the joint SNIa/BAO/CMB analysis. This results in two important conclusions:

- The FoM of the QDE EoS constraints, provided by the joint HII/BAO/CMB analysis, was found to be larger by 13 percent than those provided by the BAO/CMB joint anal-

ysis, even with the very small sample of only 25 high- z HII galaxies.

- Both the QDE and CPL EoS constraints of the HII/BAO/CMB and of the SNIa/BAO/CMB joint analyses are in excellent consistency with each other, although (as expected) the SNIa probe still provides a significantly larger FoM.

We have also performed Monte-Carlo simulations tailored to the specific uncertainties of the $L(H\beta) - \sigma$ relation and to the technical instrumental requirements of KMOS/VLT (and instruments like it). They address the important question of what is the expected increase of the FoM as a function of the number of high- z HII galaxies in the redshift windows accessible. Our previous simulations (cf. Plionis et al. 2011) did not take into account the specific error budget of our $L(H\beta) - \sigma$ relation, or the characteristics of the instruments available and of the accessible redshifts. We would like to add that cosmological analyses, like the one presented in this work, demands a thorough understanding of the interplay between observational random and systematic errors and biases, for which mock catalogues are an essential tool.

ACKNOWLEDGEMENTS

We are thankful to an anonymous referee for careful and constructive comments on the manuscript. RC, RT, ET and MP are grateful to the Mexican research council (CONACYT) for supporting this research under studentship 224117 and grants 263561, CB-2005-01-49847, CB-2007-01-84746 and CB-2008-103365-F. SB acknowledges support by the Research Center for Astronomy of the Academy of Athens in the context of the program “*Tracing the Cosmic Acceleration*”. MP acknowledges the hospitality of the KAVLI Institute for Cosmology in Cambridge, where this work was completed.

REFERENCES

- Anderson L., et al., 2014, *MNRAS*, **441**, 24
 Aubourg É., et al., 2015, *Phys. Rev. D*, **92**, 123516
 Basilakos S., Nesseris S., Perivolaropoulos L., 2013, *Phys. Rev. D*, **87**, 123529
 Bertschinger E., 2006, *ApJ*, **648**, 797
 Betoule M., et al., 2014, *A&A*, **568**, A22
 Beutler F., et al., 2011, *MNRAS*, **416**, 3017
 Blake C., et al., 2011, *MNRAS*, **418**, 1707
 Bond J. R., Efstathiou G., Tegmark M., 1997, *MNRAS*, **291**, L33
 Brouzakis N., Tetradis N., 2008, *Physics Letters B*, **665**, 344
 Chávez R., Terlevich E., Terlevich R., Plionis M., Bresolin F., Basilakos S., Melnick J., 2012, *MNRAS*, **425**, L56
 Chávez R., Terlevich R., Terlevich E., Bresolin F., Melnick J., Plionis M., Basilakos S., 2014, *MNRAS*, **442**, 3565
 Chevallier M., Polarski D., 2001, *International Journal of Modern Physics D*, **10**, 213
 Cole S., et al., 2005, *MNRAS*, **362**, 505
 Dicus D. A., Repko W. W., 2004, *Phys. Rev. D*, **70**, 083527
 Eisenstein D. J., et al., 2005, *ApJ*, **633**, 560
 Eisenstein D. J., et al., 2011, *AJ*, **142**, 72
 Erb D. K., Steidel C. C., Shapley A. E., Pettini M., Reddy N. A., Adelberger K. L., 2006a, *ApJ*, **646**, 107

- Erb D. K., Steidel C. C., Shapley A. E., Pettini M., Reddy N. A., Adelberger K. L., 2006b, *ApJ*, **647**, 128
- Freedman W. L., Madore B. F., Scowcroft V., Burns C., Monson A., Persson S. E., Seibert M., Rigby J., 2012, *ApJ*, **758**, 24
- Giraud E., 1987, *A&A*, **174**, 23
- Holz D. E., Linder E. V., 2005, *ApJ*, **631**, 678
- Holz D. E., Wald R. M., 1998, *Phys. Rev. D*, **58**, 063501
- Hoyos C., Koo D. C., Phillips A. C., Willmer C. N. A., Guhathakurta P., 2005, *ApJ*, **635**, L21
- Jaffe A. H., et al., 2001, *Physical Review Letters*, **86**, 3475
- Leitherer C., et al., 1999, *ApJS*, **123**, 3
- Linder E. V., 2003, *Physical Review Letters*, **90**, 091301
- Maseda M. V., et al., 2014, *ApJ*, **791**, 17
- Masters D., et al., 2014, *ApJ*, **785**, 153
- Matsuda Y., et al., 2011, *MNRAS*, **416**, 2041
- Melnick J., Moles M., Terlevich R., Garcia-Pelayo J.-M., 1987, *MNRAS*, **226**, 849
- Melnick J., Terlevich R., Moles M., 1988, *MNRAS*, **235**, 297
- Melnick J., Terlevich R., Terlevich E., 2000, *MNRAS*, **311**, 629
- Nesseris S., Perivolaropoulos L., 2005, *Phys. Rev. D*, **72**, 123519
- Nesseris S., Perivolaropoulos L., 2007, *JCAP*, **1**, 18
- Nesseris S., Perivolaropoulos L., 2008, *Phys. Rev. D*, **77**, 023504
- Peebles P. J., Ratra B., 2003, *Reviews of Modern Physics*, **75**, 559
- Perlmutter S., et al., 1999, *ApJ*, **517**, 565
- Planck Collaboration et al., 2015, ArXiv: astro-ph/1502.01589,
- Plionis M., Terlevich R., Basilakos S., Bresolin F., Terlevich E., Melnick J., Chavez R., 2011, *MNRAS*, **416**, 2981
- Pryke C., Halverson N. W., Leitch E. M., Kovac J., Carlstrom J. E., Holzzapfel W. L., Dragovan M., 2002, *ApJ*, **568**, 46
- Riess A. G., et al., 1998, *AJ*, **116**, 1009
- Scovaccicchi D., Nichol R. C., Bacon D., Sullivan M., Prajs S., 2016, *MNRAS*, **456**, 1700
- Shafer D. L., Huterer D., 2014, *Phys. Rev. D*, **89**, 063510
- Siegel E. R., Guzmán R., Gallego J. P., Orduña López M., Rodríguez Hidalgo P., 2005, *MNRAS*, **356**, 1117
- Spergel D. N., et al., 2007, *ApJS*, **170**, 377
- Suyu S. H., et al., 2012, ArXiv: astro-ph/1202.4459,
- Suzuki N., et al., 2012, *ApJ*, **746**, 85
- Terlevich R., Melnick J., 1981, *MNRAS*, **195**, 839
- Terlevich R., Terlevich E., Rosa-González D., Silich S., 2003, in E. Perez, R. M. Gonzalez Delgado, & G. Tenorio-Tagle ed., *Astronomical Society of the Pacific Conference Series Vol. 297, Star Formation Through Time*. p. 149
- Terlevich R., Terlevich E., Melnick J., Chávez R., Plionis M., Bresolin F., Basilakos S., 2015, *MNRAS*, **451**, 3001
- Vernet J., et al., 2011, *A&A*, **536**, A105
- Wang Y., Mukherjee P., 2006, *ApJ*, **650**, 1
- Wang Y., Holz D. E., Munshi D., 2002, *ApJ*, **572**, L15